Influence of Controlled Fluid Shear on Nucleation Rates in Glycine Aqueous Solutions

*Carol Forsyth, Paul Mulheran, Claire Forsyth, Mark D. Haw, Iain S. Burns and Jan Sefcik**

Department of Chemical and Process Engineering, University of Strathclyde, 75 Montrose Street, Glasgow, G1 1XJ, United Kingdom

The nucleation of glycine was investigated in supersaturated aqueous solutions exposed to well-controlled fluid shear under isothermal conditions. Shear rates between $25s^{-1}$ and $1000s^{-1}$ were studied using Couette and capillary flow devices. Induction times were obtained from imaging, transmission and scattering measurements or visual monitoring. Great care was taken to eliminate any seeding in order to avoid secondary nucleation preceding formation of first crystals through primary nucleation. The observed induction times of sheared solutions were considerably lower than those of unsheared solutions. Increasing the average shear rate $\dot{\gamma}_{avg}$ was found to reduce the induction time t_{ind} through a power law relationship:$t_{ind} \propto \dot{\gamma}_{avg}{}^{-0.61\pm 0.16}$. A detailed statistical analysis showed that the number of experimental repetitions used was sufficient to obtain statistically significant trends for the system studied. Induction times appeared to closely follow a probability distribution based on a previously published model of Jiang and ter Horst. Using their model, where the induction time is related to the rate of formation of primary nuclei and the time it takes them to grow to the size where the secondary nucleation becomes significant, it was found that both the primary nucleation rate and the growth time were strongly dependent on the shear rate imposed.

* Corresponding author
Jan Sefcik
Department of Chemical and Process Engineering
University of Strathclyde, 75 Montrose Street, Glasgow, G1 1XJ
Tel.: +44 (0) 141 548 2410
Email: jan.sefcik@strath.ac.uk

ABSTRACT: The nucleation of glycine was investigated in supersaturated aqueous solutions exposed to well-controlled fluid shear under isothermal conditions. Shear rates between $25s^{-1}$ and $1000s^{-1}$ were studied using Couette and capillary flow devices. Induction times were obtained from imaging, transmission and scattering measurements or visual monitoring. Great care was taken to eliminate any seeding in order to avoid secondary nucleation preceding formation of first crystals through primary nucleation. The observed induction times of sheared solutions were considerably lower than those of unsheared solutions. Increasing the average shear rate $\dot{\gamma}_{avg}$ was found to reduce the induction time t_{ind} through a power law relationship: $t_{ind} \propto \dot{\gamma}_{avg}^{-0.61 \pm 0.16}$. A detailed statistical analysis showed that the number of experimental repetitions used was sufficient to obtain statistically significant trends for the system studied. Induction times appeared to closely follow a probability distribution based on a previously published model of Jiang and ter Horst. Using their model, where the induction time is related to the rate of formation of primary nuclei and the time it takes them to grow to the size where the secondary nucleation becomes significant, it was found that both the primary nucleation rate and the growth time were strongly dependent on the shear rate imposed.

INTRODUCTION

Crystallisation is vital to many natural and industrial processes. It is widely used for separation and purification in industries such as chemicals, food and pharmaceutical; more than 90% of pharmaceutical products make use of crystalline solids as part of their manufacturing[1]. Nucleation is of fundamental importance in determining product crystal quality, however, at present it is poorly understood mechanistically and therefore the design and scale-up of processes involving nucleation presents formidable scientific and engineering challenges. Consequently, the design, operation and control of industrial applications of crystallisation are often based on trial and error or empirical correlations. An improved understanding of nucleation and the effects of relevant process parameters on nucleation pathways and resulting kinetics is therefore necessary to better design and optimise industrial applications of crystallisation.

Nucleation is the first step in the formation of a new crystalline solid phase from solution. Nuclei are particles of a given solid phase with a sufficient size to be thermodynamically stable in a solution at given supersaturation and temperature and therefore can grow by incorporating solute molecues from surrounding supersaturated solution. Nucleation is affected by supersaturation and temperature, but it can also be affected by other external factors such as agitation[2-5], mechanical shock and friction [6-9], electric and magnetic fields[10, 11], electromagnetic radiation[12], gravity[13] and ultrasound[14, 15]. Nucleation can be classed as either primary or secondary. Primary nucleation occurs in the absence of any particles of the same crystalline phase. Secondary nucleation occurs due to the presence of existing particles of the same crystalline phase[15].

In industrial processes, fluid shear is widely encountered, for example through agitation in a vessel, or transport through pipes. The role of fluid shear on the nucleation of low to medium molecular weight organic compounds from solution has not been well studied to date, with studies often focusing on larger protein molecules[16-19] or polymers[20, 21]. Agitation by a magnetic stirring bar has been reported to enhance the nucleation of various small organic compounds, including glycine[22], L-glutamic acid[23], butyl paraben[24] and carbamazepine[25]; however, shear rates are difficult to quantify in such an arrangement due to irregular motions and interactions of the stirring bar with the bottom of the vial. In order to study effects of fluid flow on nucleation in a systematic and quantitative way, well-controlled and ideally uniform flow fields are clearly advantageous. An example of a well-controlled and quantifiable shear flow is cylindrical Couette flow. Nucleation studies using such a flow have shown that increased shear rates lead to higher nucleation rate of butyl paraben[24]. Well-controlled and quantifiable shear can also be achieved using laminar capillary flow. Oscillatory flow in capillary tubes has been shown to enhance nucleation of insulin[16]. Increased flow velocities were found to result in increased nucleation rates and improved yields compared to stationary solutions. Fluid shear could potentially enhance molecular alignment or cluster aggregation and improve mass transfer, resulting in higher nucleation rates[22, 24]. The impact of shear on nucleation, however, is not always clear cut in literature and depends on the nature of the crystallising system. Shear has been found to promote nucleation of lysozyme in some systems [17, 18], however, this is not the case for anti-solvent induced lysozyme crystallisation in which interfacial instabilities, with regions of elevated supersaturation, appear to play an important role in nucleation [26]. Shear was found to reduce the formation of these interfacial instabilities, and nucleation was reduced. Similar

conclusions regarding the detrimental effect shear can have on interfaces have been made in other work [19], where it was found that thaumatin nucleation in microcapillaries was reduced at increased flow rates due to the reduction of the interface's lifetime. Literature on the crystallisation of colloids also often shows conflicting results. Several reports suggest that shearing can enhance the crystallisation of colloids[27-29], while others report that it can significantly suppress it[30-32].In order to clarify the effects of shear in a systematic and controlled way, here we study the nucleation of glycine from aqueous solutions using well characterised flow geometries. We use both cylindrical Couette and capillary flow over a wide range of shear rates, in order to provide experimental data on the effect of fluid shear on the nucleation behaviour. Induction times are measured using a range of techniques (transmission and scattering measurements, imaging and visual monitoring). Due to the stochastic nature of nucleation, experiments are repeated multiple times. A statistical analysis is performed to show that this number of repetitions is sufficient for accurate trends to be deduced.

EXPERIMENTAL SECTION

Nucleation experiments were performed using two flow geometries: cylindrical Couette and capillary. Supersaturated glycine solutions were subjected to controlled flow conditions in these geometries and induction times were measured.

Flow Systems

Couette setup

A cylindrical Couette flow system was set up as shown in Figure 1. The inner cylinder was kept fixed, while the outer cylinder was rotated. We note that the fixed inner/rotating outer cylinder geometry does not result in the Taylor instabilities (Taylor vortices superimposed on laminar Couette flow), which would have occurred in a fixed outer/ rotating inner cylinder for the conditions used[33]. This means that the laminar shear rates in the gap between the two cylinders could be accurately quantified by solving the Navier-Stokes equation.

The outer cylinder had an inner diameter of 38mm and the inner cylinder (hollow) had an outer diameter of 30mm. Both cylinders were made of glass. The geometry resulted in a 4mm gap between the vertical inner and outer cylinders. The depth of solution in the gap was approximately 6cm. A gap of 1-2 mm was kept between the base of the inner and outer cylinders. Visual observations showed that nucleation began in solution contained within the vertical gap between the cylinder walls. Further experiments have been carried out that involved using an inner cylinder with a smaller diameter, and a similar base gap of 1-2mm. Since an inner cylinder with a smaller diameter resulted in a larger gap between the inner and outer vertical cylinders, larger rotational rates had to be used to achieve the required shear

rates. Despite higher rotational rates (and therefore higher shear rates in the gap at the bottom), nucleation occurred more slowly. This confirmed that the controlled shear in the vertical gap between the cylinder walls had the main effect on nucleation. A Perspex lid was present to minimise evaporation. The outer cylinder was rotated by means of a motor powered by a variable d.c. power supply. A digital tachometer was used to measure the rotational speed.

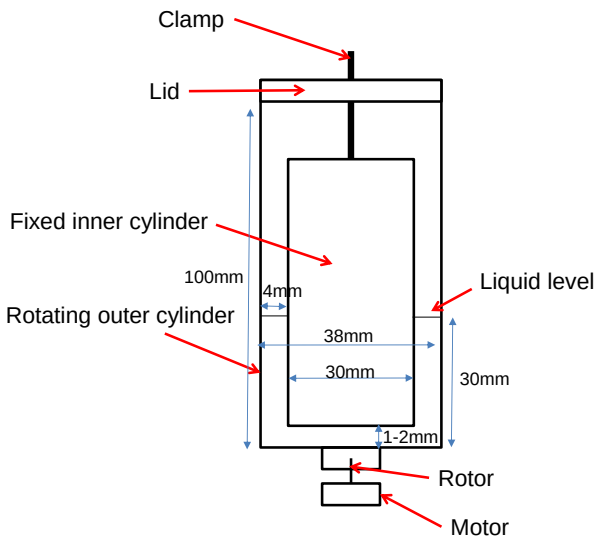

Figure 1. Couette setup.

The velocity, v, profile across the gap of the Couette cell was approximated by solving a momentum balance across the system (from the Navier-Stokes equation) assuming steady state operation.

$$\frac{\partial v}{\partial t} = \eta \left[\frac{\partial}{\partial r}\left(\frac{1}{r}\frac{\partial}{\partial r}(rv)\right)\right] = 0 \qquad \text{Equation (1)}$$

Here r is radial position, η is kinematic viscosity and t is time.

The velocity across the gap could therefore be approximated as:

$$v(r) = 2\pi N r_{out} \frac{r_{out}}{r} \frac{\left(1-\frac{r^2}{r_{in}{}^2}\right)}{\left(1-\frac{r_{out}{}^2}{r_{in}{}^2}\right)} \qquad \text{Equation (2)}$$

Here N is the rotational speed, r_{out} is the radius of the outer cylinder and r_{in} is the radius of the inner cylinder. In addition to calculating velocity profiles derived from the Navier Stokes equation (Equation 2), the velocity profiles for the experimental conditions used here were also estimated by assuming a perfectly linear velocity profile. The maximum difference between the two methods was 10%.

The shear rate, $\dot{\gamma}$, was therefore:

$$\dot{\gamma}(r) = \frac{dv(r)}{dr} = 2\pi N r_{out} \frac{\left(-\frac{1}{r^2}-\frac{1}{r_{in}{}^2}\right)}{\left(\frac{1}{r_{out}}-\frac{r_{out}}{r_{in}{}^2}\right)} \qquad \text{Equation (3)}$$

The average shear rate across the gap, $\dot{\gamma}_{avg}$, was calculated from:

$$\dot{\gamma}_{avg} = \frac{1}{r_{out}-r_{in}} \int_{r_{in}}^{r_{out}} \dot{\gamma}(r)\, dr = \frac{2\pi N r_{out}}{r_{out}-r_{in}} \qquad \text{Equation (4)}$$

Radial variations in shear rate were less than 25% for experimental conditions used here. Using the velocity of the rotating outer cylinder and the gap length between the cylinders, the Reynolds number, Re, varied from 300 to 3000 (Equation 5). The kinematic viscosity was obtained by experiment and compared well to correlations found in literature[34].

$$Re = \frac{(2\pi N r_{out})(r_{out}-r_{in})}{\eta} \qquad \text{Equation (5)}$$

Critical Reynolds numbers depend on the geometry used and can be found experimentally [35]. To ensure that the critical Reynolds number for the conditions used in the experiments was not surpassed, rheoscopic fluid (suspension of mica platelets that align with the flow) and dye injections were used in the Couette, and the flow was visualised for the rotational speeds used in the experiments. Even at the highest rotational speed used, the flow did not show significant instabilities when the outer cylinder was rotated. This suggests that flow in the gap between cylinders is streamline for the conditions studied. We note that large instabilities were observed when the inner cylinder was rotated and the outer cylinder was kept fixed, in agreement with what would be expected from theory[33].

Capillary setup

A capillary flow system was set up as shown in **Error! Reference source not found.**. 12.5 metres of Nalgene PVC tubing (2mm ID, 4mm OD) was attached to a syringe. Due to the length of tubing, it was coiled around a cylindrical vessel.

The syringe was attached to a programmable syringe pump (Cole Parmer 74905-54). This allowed flow rates to be controlled and it could be operated in infusion and withdrawal modes sequentially, to result in continuous, periodic 'square wave' operation. To achieve this, the tube was filled with solution and a chosen volume of fluid (10ml), which corresponded to ~3.2m of tube, was withdrawn into the syringe and then infused back into the tube continuously; this resulted in the fluid passing back and forth along the tube periodically. The syringe pump bar pulled the syringe plunger at a constant velocity,

withdrawing fluid back into the syringe, resulting in steady flow at a fixed velocity along the tube in a negative direction; this was then followed by the syringe pump bar pushing the syringe plunger at a constant velocity, infusing fluid back into the tube, resulting in steady flow at a fixed velocity along the tube in a positive direction. This was repeated, resulting in continuous, periodic flow back and forth along the tube in 'square waves'.

The frequency was low (5 cycles per minute) and the amplitude was large ($0.13ms^{-1}$ for the lowest shear rate used here and $0.52ms^{-1}$ for the largest shear rate used here). The time taken for the syringe pump to reach its operating velocity was negligible compared to the duration at which it ran at its constant operating velocity. A lag time of around 1s occurred when the syringe pump switched between infusion and withdrawal modes; this time was significantly greater than the relaxation time of the fluid.

Due to the 'square wave' nature of the operation, shear rates were calculated on the assumption of laminar flow of a Newtonian fluid in a horizontal, cylindrical pipe. Although the tubing was coiled, the diameter of the coil was kept large (10cm) compared to the diameter of the tubing. Entry lengths[35] (length of pipe before flow becomes fully developed) were found to be negligible compared with the length of the tube (and half length of square waves).

The parabolic velocity profile for Newtonian, laminar flow in a cylindrical pipe can be expressed as:

$$v(r) = 2v_{avg}\left(1 - \frac{r^2}{\mathcal{R}^2}\right) \qquad \text{Equation (6)}$$

Here v_{avg} is the average velocity, r is distance from the pipe centre and $\mathcal{R}$ is the pipe's inner radius.

The shear rate magnitude at distance r from the pipe centre was therefore:

$$\dot{\gamma}(r) = \frac{dv(r)}{dr} = \frac{4rv_{avg}}{\mathcal{R}^2} \qquad \text{Equation (7)}$$

The average shear rate across the tube can be found:

$$\dot{\gamma}_{avg} = \frac{1}{\mathcal{R}-0}\int_0^{\mathcal{R}} \dot{\gamma}(r)\, dr = \frac{2v_{avg}}{\mathcal{R}} \qquad \text{Equation (8)}$$

The maximum shear rate, $\dot{\gamma}_{max}$, occurring at the walls was:

$$\dot{\gamma}_{max} = 2\dot{\gamma}_{avg} \qquad \text{Equation (9)}$$

Using the average velocity of the fluid and the tube diameter, the Reynolds, Re, number varied from 250 to 1000 indicating streamline flow, using

$$Re = \frac{v_{avg} 2\mathcal{R}}{\eta} \qquad \text{Equation (10)}$$

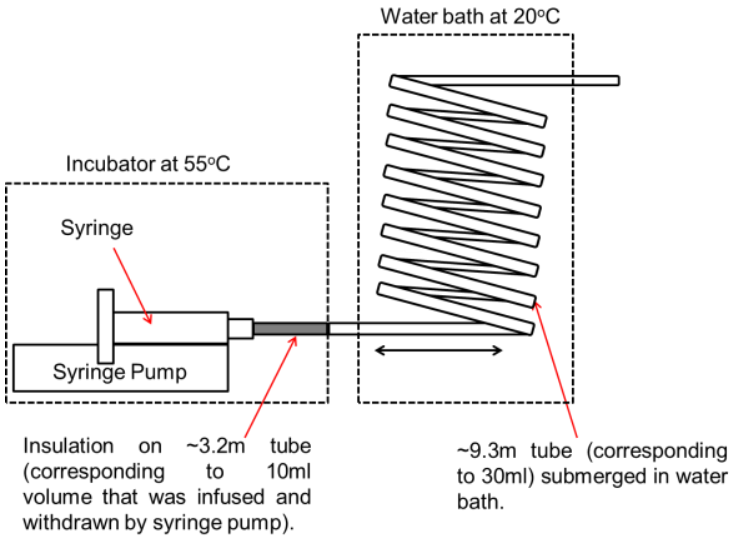

Figure 2. Capillary setup.

Since the solubility of glycine in water increases with increasing temperature, the syringe and the length of tube that corresponded to the volume of fluid that was withdrawn and infused by the syringe pump (3.2m corresponded to 10ml volume) were kept incubated and insulated (Figure 2). This was to ensure that solution that was entering and leaving the syringe during operation was kept at a temperature that would result in the solution being undersaturated. Fluid in the length of tube that was not incubated and insulated (~8.3m) was cooled and became supersaturated. Incubating and insulating the solution that was entering and leaving the syringe was necessary since entering and exiting the syringe was found to strongly enhance nucleation, leading to blockages if solution entering and leaving was supersaturated.

Experiment Monitoring

Couette experiments were monitored by one of two methods: (1) simultaneous measurements of static light scattering at the scattering angle of 90^{o} and transmitted light intensity; (2) imaging the nucleation process and then analysing the images. The layout is given in Figure 3. Scattering and transmission data were obtained using a custom-built instrument, similar to one used previously for in situ monitoring of stirring effects on crystallisation of carbamazepine[25].

The beam from a helium-neon laser (Thorlabs HRP170; 17 mW; beam diameter ~ 1 mm) was directed through the Couette cell. Weak reflections of the beam from beam sampler plates

were incident on photodiodes (Thorlabs PDA36A-EC) to measure the intensities of incident and transmitted beams. An avalanche photodiode (Hamamatsu APD C5460) was used to measure the intensity of light scattering at 90º. Signals were digitised by a data-acquisition card (National Instruments PCI-6221) and recorded using LabVIEW. A camera (Logitech Webcam 300) was used for imaging of ambient light scattered by incipient crystals. The mean pixel intensity of a chosen area in the images was calculated and plotted as a function of time. Transmission/ scattering measurements and images were recorded every second.

When the induction time was reached, solutions became turbid over a short timescale (as short as around 10s), leading to a sharp increase in scattering, a decrease in transmission and an increase in mean pixel intensity. Induction times were obtained by finding the point of inflection of the rising signals; the three measurement methods were found to give consistent results (inflections occurred at identical times for simultaneous scattering and transmission measurements, and for imaging, the times where inflections occurred were of a similar time range to those obtained through transmission/ scattering measurements). Induction times for capillary experiments were obtained by visual monitoring. The induction times measured through this qualitative method would have had increased uncertainty over the quantitative methods used for Couette experiments.

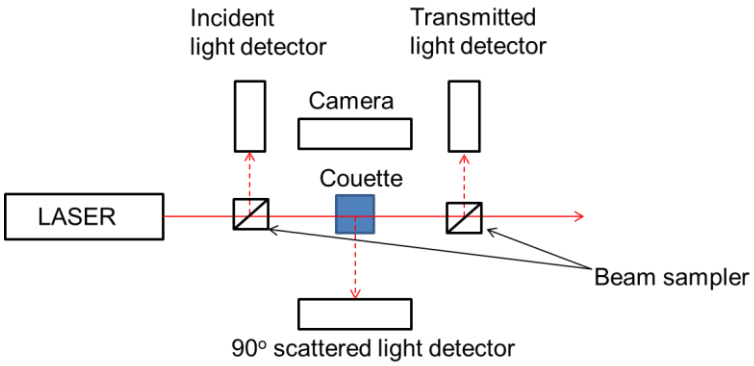

Figure 3. Monitoring equipment setup.

Solution Preparation

Glycine (CAS Number 56-40-6) of ≥ 99% purity was purchased from Sigma Aldrich (item G8898) and used without further purification. Two concentrations, c, of solution were prepared by dissolving glycine in deionised water- 307g glycine/kg water and 325g glycine/kg water. During experiments, these solutions were cooled to 20°C and 23°C respectively. The solubility, c*, of glycine was 219g glycine/kg water at 20°C and 232g glycine/kg water at 23°C[36].Cooling therefore resulted in a supersaturation, S, of 1.4 for both solutions, where

$$S = \frac{c}{c^*} \qquad \text{Equation (11)}$$

Solutions were prepared in sealed glass bottles and were stirred at 55°C for 24hours to ensure that glycine was fully dissolved.

Experimental Procedure

Couette setup

15ml undersaturated solution (in incubator at 55^{o}C) was filtered using preheated 0.2μm SFCA disposable syringe filters (with the exception of 250rpm imaging experiments for which solutions were unfiltered) into a preheated Couette cell by syringe. The filters, syringe and Couette cell were preheated to 55^{o}C in the incubator, and the filtration procedure took place inside the incubator to minimise the rate of heat loss.

The filled Couette cell was removed from the incubator and attached to the monitoring instrument. A lid was secured to minimise evaporation and the solution was left to cool in the surrounding air (23^{o}C) for 30mins in order to reach ambient temperature and the desired level of supersaturation. There was no cylinder rotation during cooling. During cooling, a fan was used to speed up heat transfer. The temperature profile of the solution during cooling was measured to validate that the 30 minute cooling time was sufficient to ensure that the solutions had reached the desired temperature after this time. The ambient temperature remained constant so the solution remained isothermal once it had cooled to 23^{o}C. Once the solution cooling period had finished, the fan was switched off and the motor and monitoring equipment were started.

Since shearing of the solutions took place under isothermal conditions (the temperature of the solution was equal to the temperature of its surroundings), the effect of laminar shear on induction times was not linked to heat transfer.

Rotational speeds (50rpm, 125rpm, 250rpm or 500rpm) were measured using the digital tachometer and the voltage was adjusted to obtain the desired rotational speed. Once the solution had become visibly turbid, the motor and monitoring equipment was switched off. Data were then analysed to obtain induction times. Induction times were also obtained for

experiments that involved no shearing i.e. 0rpm. This was done visually as only a small number of crystals formed in unsheared solutions (fewer than 5, typically 1 or 2) which meant solutions did not become turbid. For induction time measurements, t=0 is defined as the time at which the motor was started and cylinder rotation began. This happened after the solution had cooled to 23^{o}C and therefore reached the desired level of supersaturation i.e. t=0 was 30 minutes after the filled Couette cell was removed from the incubator.

Capillary setup

50ml undersaturated solution was filtered (using 0.2μm SFCA filters) into a preheated syringe and the syringe was attached to the syringe pump. The pump, syringe and the adjacent length of tubing that corresponded to the volume of solution that was withdrawn and infused by the syringe pump (a 10ml volume was used which equated to approximately 3.2m of tubing) were kept insulated at 55^{o}C so that the solution that entered and left the syringe during continuous operation remained undersaturated. The remaining tubing was submerged in a water bath at 20^{o}C (see Figure 2). 50ml solution was infused from the syringe through the tubing; the first 10ml was discarded leaving 40ml in the tube. The 30ml solution in the non-incubated/ uninsulated length of tubing was left to cool in the water bath (20^{o}C) for 10mins. Once the solution had cooled, the syringe pump was operated in a continuous mode whereby 10ml solution was passed back and forth periodically at a chosen flowrate (25ml/min, 50ml/min or 100ml/min) while staying isothermal at 20^{o}C in the non-incubated/ uninsulated length of tube. The solution in the tube was monitored visually and the induction time was noted. Induction times were also obtained for experiments that involved no shearing, i.e. the flowrate was 0ml/min. For induction time measurements, t=0 is defined as

the time at which the syringe pump was started and flow back and forth along the tube began. This happened after the solution in the uninsulated length of tube had cooled to 20^{o}C and therefore reached the desired level of supersaturation i.e. t=0 was 10 minutes after the tube was submerged in the water bath and infused with undersaturated (55^{o}C) solution.

RESULTS AND DISCUSSION

Figure 4 shows the induction times obtained at each rotational speed for Couette flow. By increasing the rotational speed (and therefore flow velocity and shear rate), smaller mean induction times were obtained. At 50rpm, the induction times obtained were approaching the induction times measured for unsheared solutions, however, at higher rotational speeds, the induction times measured were considerably smaller. Values obtained from both measurement methods ((1) simultaneous measurements of static light scattering at the scattering angle of 90^{o} and transmitted light intensity; (2) imaging the nucleation process and then analysing the images) overlapped and had similar mean values. The simultaneous scattering and transmission measurements gave identical induction times; since solutions quickly became very turbid, sensitivity differences between the detection methods were not very important.

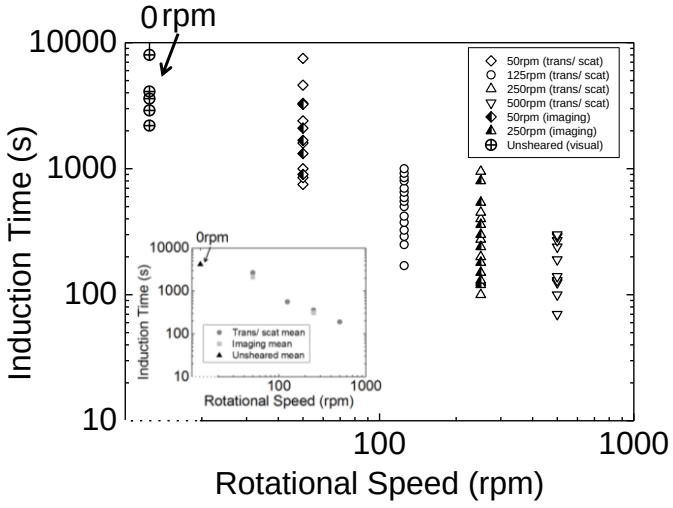

Figure 4. Induction times measured using Couette setup.

Figure 5 shows the induction times obtained at each flow rate used for capillary flow. By increasing the flow rate (therefore flow velocity and shear rate), smaller mean induction times were obtained. The induction times obtained for all flow rates used were considerably smaller than those of unsheared solutions.

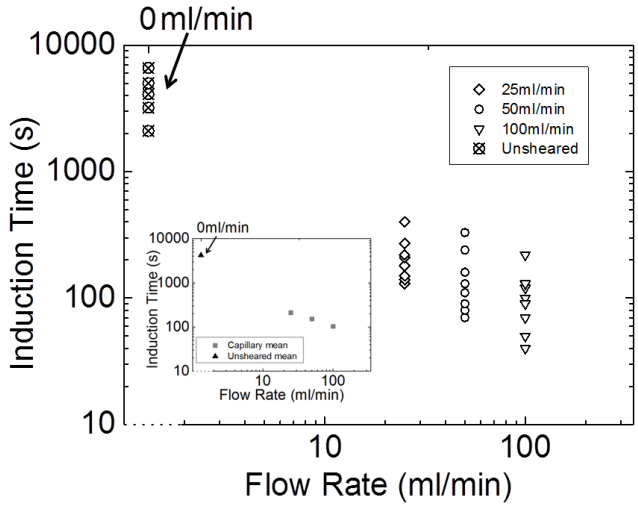

Figure 5. Induction times measured using capillary setup.

Figure 6 shows the mean and median of capillary and Couette results presented together as a function of average shear rate. Both flow geometries gave similar mean induction times when solutions were sheared at the same average shear rate (500rpm and 25ml/min).

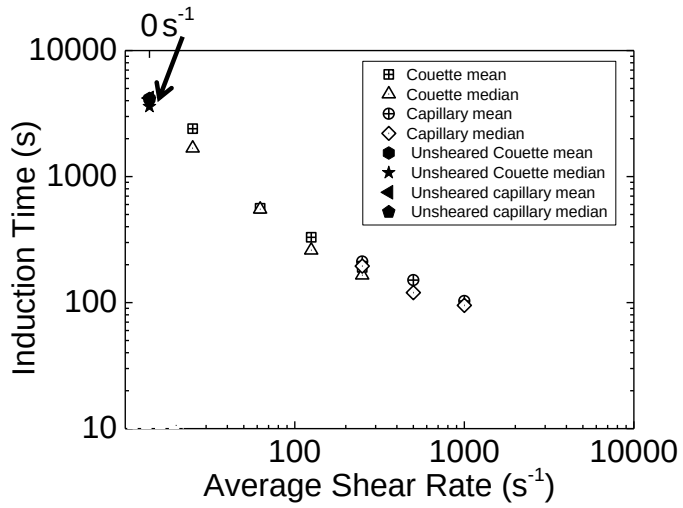

Figure 6. Mean and median induction times as function of average shear rate for Couette and capillary flows. For capillary experiments, the maximum shear rate, which occurs at the walls, would be twice the average shear rate.

Shearing was hypothesised to have an influence on both primary and secondary nucleation. Since induction times were notably smaller for higher shear conditions than for unsheared solutions, it is important to distinguish effects on primary and secondary nucleation, respectively. Preheating and filtration of solutions was done to ensure that no crystals were initially present in aqueous glycine solutions. In order to eliminate any seed crystals that were present at glass walls of Couette cylinders or in plastic capillaries, these were extensively cleaned with hot water after each experiment. No crystals have been seen after inspection under an optical microscope. In order to ensure this was indeed the case, observations were made under quiescent unsheared conditions and it was invariably seen that a small number of crystals (typically 1 or 2 after 4 hours) appear at the base of the Couette cylinder. After 4h, the largest dimension observed was 6mm, and using growth rates from literature[37] based on the same supersaturation and temperature (growth rates were also verified experimentally by

placing a seed crystal in the supersaturated solution and monitoring its growth), the longest axis would be expected to be at least 14mm if a crystal was already present at the start of the experiment. This shows that there were no crystals present in the system at the start, neither in the bulk nor on the walls exposed to the supersaturated solution. It can be therefore concluded that the crystals formed at higher shear rates were due to shear enhanced primary nucleation of a nucleus (or small number of nuclei), followed by extensive secondary nucleation. This is in agreement with work carried out by Jiang and ter Horst[38] which suggested that the crystallisation mechanism was due to the nucleation of a single parent crystal, followed by the attrition of the single parent crystal to form secondary nuclei.

For 50rpm Couette experiments, the formation of the primary nucleus/nuclei may not have been greatly shear enhanced, since induction times were fairly similar to those in unsheared solutions. Solutions sheared at 50rpm, however, became turbid, unlike unsheared solutions, so secondary nucleation was likely to still have been enhanced by the flow conditions. The rate at which turbidity increased with 50rpm experiments was lower than the other rotational speeds, which suggested slower secondary nucleation. We note that the induction time detection method for 50rpm experiments (scattering/ transmission/ imaging) and unsheared experiments (visual) differed. For 50rpm experiments, sufficient secondary nucleation had to take place before measured signals were affected, meaning that an overestimation of induction times may have occurred when comparing to unsheared solution induction times.

When solutions were not sheared, fewer than 5 crystals (usually 1 or 2) typically formed and these would have been formed through primary nucleation, as discussed above. However, when solutions were sheared, a very large number of crystals formed in close succession,

causing solutions to rapidly go turbid. The large number of crystals formed over such a short timescale is most likely due to the secondary nucleation, rather than a sudden, large increase in primary nucleation[15, 38-40].

Distributions of induction times

The distributions of induction times obtained were further investigated to gain better understanding of underlying nucleation phenomena. There have been several approaches in previous literature to analyse induction time distributions based on probabilistic arguments.

A simple approach is to assume that the induction times are log-normally distributed, since log-normal distributions have been often observed to fit probabilistic outcomes of various natural phenomena[41]. In this case, the cumulative distribution of the logarithm of induction times follows the cumulative distribution function:

$$Q(\mathrm{t}) = \frac{1}{2}\left[1 + \mathrm{erf}\left(\frac{\log(t) - \overline{\log(t)}}{\sigma\sqrt{2}}\right)\right] \qquad \text{Equation (12)}$$

Here, erf is the error function, $\overline{\log(t)}$ is the mean of the log induction time and σ is its standard deviation. These data are calculated for each set of induction times recorded at each experimental condition (see Figure 6). However, even if a log-normal distribution described induction time data well, there is no clear way to deduce further information about underlying physical phenomena from the shape of a distribution of induction times.

In order to obtain quantitative insight into nucleation phenomena from experimentally observed distributions of induction time, we consider a model proposed by Jiang and ter Horst[38] In the model it is assumed that, due to the stochastic nature of nucleation in small

volumes, the probability of forming a particular number of crystals over a time interval followed a Poisson distribution[38,42]. A Poisson distribution was appropriate because the nucleation events are independent and should occur at a constant average rate over the time interval.

The cumulative distribution function of nucleation times, which is the likelihood that the first nucleation event occurs up to time t_n, is

$$P(t_n) = 1 - exp(-JVt_n) \qquad \text{Equation (13)}$$

Here J is the nucleation rate per unit volume and V is the volume of the solution. For Couette experiments, a volume of 15ml was used. For capillary experiments, a volume of 30ml, which corresponded to the volume of solution in the uninsulated section of capillary, was used. The nucleation rate in general depends on supersaturation and temperature, and it may also vary depending on other process parameters, such as the shear rate.

The induction time t that is observed in the experiments is the time at which the solution becomes clouded by many crystals. The second element of the Jiang and ter Horst model is that the first nucleation event (due to primary nucleation) occurring at time t_n leads to the observed clouding at a later time $t = t_n + t_g$. Here t_g is interpreted as the growth time for further crystals, which are rapidly produced through secondary nucleation following the creation of the first crystal by primary nucleation, to grow to a sufficient size to be observed. Thus we find the proportion of observations made by time t is

$$P(t) = 1 - \exp\big(-JV(t - t_g)\big) \qquad \text{Equation (14)}$$

Experimentally, for a given set of conditions we observe a number of induction times t_i, $i = 1,2, \ldots \mathrm{M}$, which we order from shortest to longest. The observed cumulative probability distribution of induction times $O(t)$ which is to be compared to Eqn. (14) is then

$$O(t_i) = \frac{i}{M} \qquad \text{Equation (15)}$$

The data in the form of Eqn. (15) are used to find the best fit values for J and t_g in Eqn. (14) for each experimental condition; this was done using the least squares fitting procedure in Matlab's curve fitting toolbox. When best estimates for J and t_g are obtained at various shear rates, we can determine whether nucleation rates and growth times show dependence on shear rates under conditions investigated here.

In Figure 7 we show experimental data for the Couette and capillary systems, respectively, together with log-normal distribution curves from Eqn. (12) using the mean and standard deviation of the log times for each set of data, and also with the best fit of the Jiang and ter Horst model, Eqn. (14).

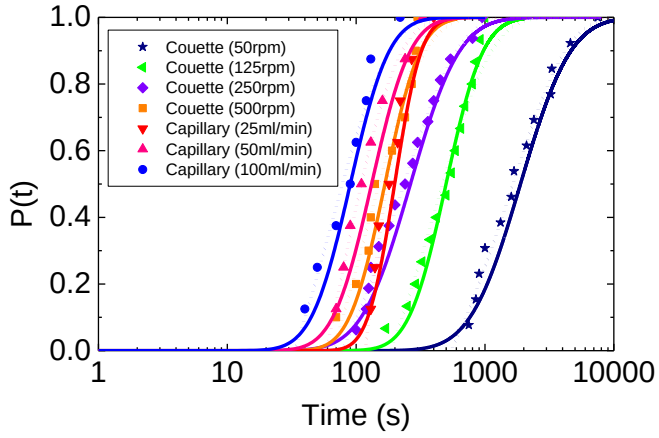

Figure 7. Cumulative distribution functions for induction times from Couette and capillary setups. Symbols represent experimental data, dashed line is the best fit for the model of Jiang and ter Horst (Eqn. (14)) and solid line is the log-normal distribution (Eqn. (12)).

While log-normal distributions agree with experimental data reasonably well, the functional form of the model by by Jiang and ter Horst does seem to be better suited to describing our data under all conditions investigated here (see Figure 8).

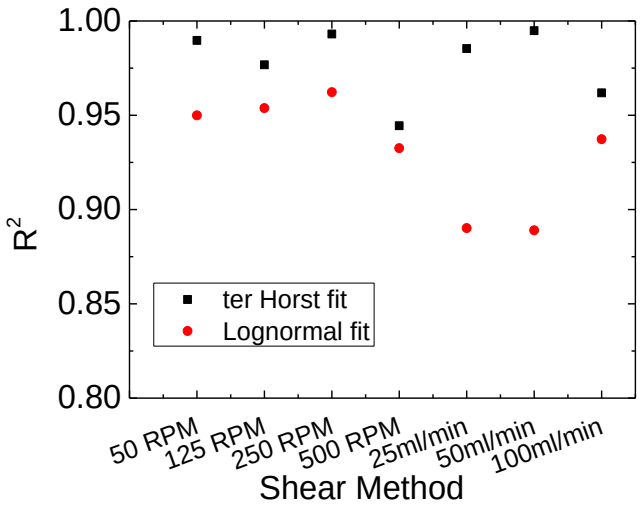

Figure 8. Coefficients of determination for the best fit of the model by Jiang and ter Horst and for the log-normal model.

Nucleation rates J and growth times t_g obtained from the best fit of the model by Jiang and ter Horst fit are shown in Figure 9. As we have already seen that the observed induction times decrease with increasing shear rate (cf. Figure 6), it would be expected that the nucleation

rate increases with increasing shear rate, and/or the growth time decreases with increasing shear rate. As we can see in Figure 9, nucleation rates increase fairly sharply at lower shear rates (<100 s^{-1}) followed by a slower increase at higher shear rates (>100 s^{-1}), and there is a good agreement between values obtained from Couette and capillary measurements. It can be seen that nucleation rates can be enhanced by at least one order of magnitude by laminar shear flow in the flow setups used here. The increase of nucleation rate with increasing shear rate, as shown in Figure 9, could be explained by several possible factors such as improved mass transfer, better molecular alignment or enhanced cluster aggregation[22, 24], although it is not yet clear what the most likely mechanism is in this system.

It can be also seen in Figure 9 that growth times decrease significantly with increasing shear rates. This can be due to enhanced mass transfer to the growing crystals as well as due to secondary nucleation increasing with increasing the shear rate, meaning that a detectable amount of crystals formed more quickly; if there are more secondary nuclei, they will not have to grow to as large a size to be detected.

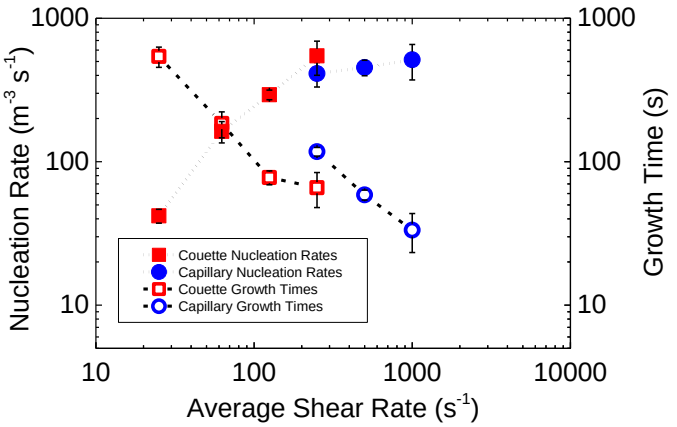

Figure 9. Nucleation rates J and growth times t_g estimated from the best fit of the model by Jiang and ter Horst. Error bars represent 95% confidence intervals.

Statistical trends and the impact of sample size

Recent literature suggests that due to the stochastic nature of nucleation, a large number of repetitions (on the order of 100) should be carried out to obtain accurate results[24, 38, 40, 42, 43]. We have carried out a detailed statistical analysis of our experimental data and found that far fewer repetitions were sufficient to deduce reliable trends for how the nucleation rates vary with shear rate for the system investigated here.

Our approach is to generate model datasets of varying sample size at each shear rate, using the bootstrapping or Monte Carlo simulations described below. We then fit a linear regression to the log(induction time) versus log(average shear rate) plots of these model data. The slope

of the regression will vary from one model dataset to another, and we are interested to learn how the mean and standard deviation of this slope depends on sample size. As we show below, we find that the number of experimental repetitions we have performed in this work is indeed sufficient to obtain statistically reliable results. Furthermore, we also calculate the best fit slope for our experimental data and its confidence interval.

Bootstrapping

Bootstrapping of the data was done to estimate the reliability of the regression slopes obtained from linear least squares fits to the log(induction time) data as a function of log(average shear rate)[44]. The bootstrapping approach has proved useful in estimating standard deviations in other nucleation systems[45]. Here we randomly resample the experimental data (with replacement so that a given data point can be re-selected) for each set of conditions and calculate the slope from the least squares fit for the resampled data. This was repeated 400 times and the mean slope and standard deviation were found. Full and partial bootstraps were done. For the full bootstrap, the number of resamples was equal to the number of measurements in each data-set taken at the various experimental conditions. For partial bootstraps, the number of resamples was varied from 1 to 10.

Monte Carlo Simulations

Monte Carlo simulations were carried out by assuming that the induction times followed the Jiang and ter Horst model; parameters for this (nucleation rate and growth time) were obtained for each set of data as described above. For each modelled distribution, a large

number of samples was drawn in the usual Monte Carlo procedure, allowing the effect of sample size to be investigated more robustly than in the bootstrap method.

As with the bootstrapping, the slope from the least squares fit of the sampled data was calculated for each simulated data set, and the procedure was repeated 400 times. From the repetitions, the mean slope and the corresponding standard deviation were found.

Results

As expected, the standard deviation in the calculated slopes was found to decrease with increasing number of samples, as shown in Figure 10. Although Monte Carlo simulations showed that increasing the number of repetitions to 100 would ensure much lower uncertainties, as expected, the statistical significance of the observed trend could be established with far fewer repetitions.

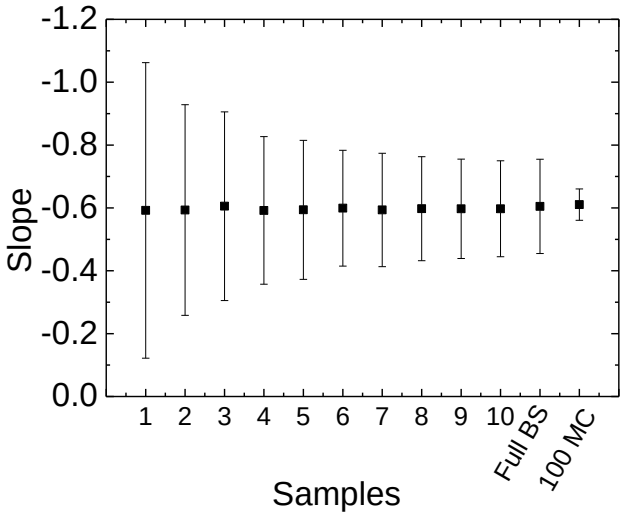

Figure 10. Slopes found from bootstrapping (BS) (1-10 resamples and full) and 100 sample Monte Carlo (MC) simulation. Based on experimental data from Couette (excluding 50rpm) and capillary setups. Error bars represent 2 standard deviations.

The slope values obtained through each method depended on which data were included in the analysis; since distributions of induction times for 50rpm (the lowest rotational speed used) overlapped significantly with those for unsheared solution, fits were done including and excluding these. The slopes and standard deviations found from full bootstraps of different data sets are shown in Table 1. Importantly, the slopes found were always negative. This confirmed that it was valid to conclude that increasing shear rates were associated with smaller induction times for the system investigated here.

Table 1. Slopes and standard deviations from full bootstraps of various data sets.

Data used	Slope from full bootstrap	2 Standard Deviations
Couette	-1.07	0.22
Couette excluding 50rpm data	-0.79	0.28
Capillary	-0.57	0.32
Couette and capillary	-0.81	0.12
Couette and capillary excluding 50rpm data	-0.61	0.16

Excluding the 50rpm data had a significant effect on all slopes. which suggested that nucleation may have been occurring by a different mechanism for these conditions compared to the other Couette and capillary data. The 50rpm induction times may also have been overestimated due to the slower rate of secondary nucleation that occurred for these experiments, compared to higher rotational speeds. Sufficient secondary nucleation had to take place before measured signals were affected enough to obtain clear induction times.

When 50rpm data were excluded, slopes were within confidence intervals of each other for Couette and capillary results, as shown in Figure 11. This suggested that shear enhanced primary nucleation may have been occurring through similar mechanisms in the both flow setups. The slopes found from analyses based on multiple Couette and capillary data sets had reasonably low standard deviations, particularly when the number of samples exceeded 5. This indicated that the slopes obtained reliably represented the trend of the experimental data. Standard deviations were larger when analyses were based on fewer data sets or a smaller number of samples per data set, as expected.

The slopes obtained from Monte Carlo simulations compared closely to the slopes obtain from bootstrapping the data. This suggested that the distributions assumed matched the experimental data well.

The slopes (and therefore powers in the power law dependence of the mean induction time on the average shear rate) found therefore suggested that when anomalous data (50rpm) were excluded, $t_{ind} \propto \dot{\gamma}_{avg}{}^{-0.61\pm 0.16}$ based on a full bootstrap to the data.

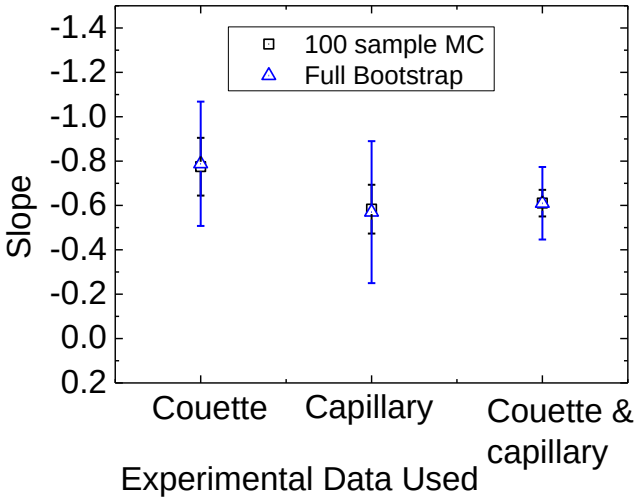

Figure 7. Slopes found for Couette and capillary data (excluding 50rpm data) using full bootstraps and 100 sample Monte Carlo simulation model). Error bars represent 2 standard deviations.

CONCLUSIONS

The nucleation of glycine was investigated in supersaturated aqueous solutions exposed to well-controlled fluid shear under isothermal conditions. Well characterised flow geometries based on Couette and capillary setups were used over a wide range of average shear rates ($25s^{-1}$ and $1000s^{1}$) and induction times were estimated using a range of techniques, including imaging, transmission and scattering measurements and visual monitoring. Due to the stochastic nature of nucleation, experiments were repeated multiple times and a statistical analysis was performed to show that this number of repetitions was sufficient for accurate trends to be deduced. Great care was taken to eliminate any seeding in order to avoid secondary nucleation preceding formation of first crystals through primary nucleation.

Induction times obtained under shearing in Couette or capillary setups were found to be considerably lower than those in unsheared solutions. Distributions of induction times appeared to closely follow a distribution based on a previously published model by Jiang and ter Horst. Using their model, where the induction time is related to the rate of formation of primary nuclei and the time it takes them to grow to the size where the secondary nucleation becomes significant, it was found that both the primary nucleation rate and the growth time were strongly dependent on the shear rate imposed. Moreover, increasing the average shear rate reduced the mean induction time in a power law relationship: $t_{ind} \propto \dot{\gamma}_{avg}^{\ -0.61\pm 0.16}$.

Using the model of Jiang and ter Horst, we found that the primary nucleation rate increases and at the same time, the growth time decreases with increasing shear rate. The nucleation rates increase fairly sharply at lower shear rates (<100 s^{-1}) followed by a slower increase at higher shear rates (>100 s^{-1}), and there is a good agreement between values obtained from

Couette and capillary setups. The nucleation rates are enhanced by at least one order of magnitude by laminar shear flow in the flow systems studied.

AUTHOR INFORMATION

Corresponding Author
*Tel.: +44 (0) 141 548 2410. Email: jan.sefcik@strath.ac.uk

ACKNOWLEDGMENTS

We would like to thank James Murphy for his invaluable technical assistance and advice. The Carnegie Trust for the Universities of Scotland is acknowledged for funding the PhD scholarships for Carol Forsyth and Claire Forsyth.

NOTATION

c = concentration of glycine

c* = solubility of glycine

erf = error function

J= nucleation rate

$\overline{\log(t)}$ = mean logged induction time

N= rotational speed

$N_{crystals}$= number of crystals formed in the solution volume

$P(t)$ = cumulative distribution of nucleation times in the ter Horst model

$Q(\mathrm{t})$ = cumulative distribution of nucleation times for the lognormal model

$\mathcal{R}$ = pipe's inner radius

R^2 = coefficient of determination

r = radial position

r_{in}= radius of inner cylinder

r_{out}= radius of outer cylinder

S= supersaturation

t= time

t_n= nucleation time in the ter Horst model

t_g= growth time

t_i= experimentally observed induction time

V= solution volume

v= velocity

v_{avg} = average velocity

$\dot{\gamma}$= shear rate

$\dot{\gamma}_{avg}$= average shear rate

$\dot{\gamma}_{max}$ = maximum shear rate

η= kinematic viscosity

σ= standard deviation of log induction time

REFERENCES

(1) Erdemir, D.; Lee, A. Y.; Myerson, A. S., Nucleation of Crystals from Solution: Classical and Two-Step Models. *Accounts of Chemical Research* 2009, 42, (5), 621-629.

(2) Mullin, J. W.; Raven, K. D., Influence Of Mechanical Agitation On Nucleation Of Some Aqueous Salt Solutions. *Nature* 1962, 195, (4836), 35-&.

(3) Mullin, J. W.; Raven, K. D., Nucleation In Agitated Solutions. *Nature* 1961, 190, (477), 251-&.

(4) Nyvlt, J.; Skrivane.J; Gottfrie.J; Krickova, J., Uber Kristallisation .19. Einfluss Der Durchmischung Auf Die Breite Der Metastabilen Zone. *Collection of Czechoslovak Chemical Communications* 1966, 31, (5), 2127-&.

(5) Joshi, M. S.; Antony, A. V., Nucleation In Super-Saturated Potassium Dihydrogen Ortho-Phosphate Solutions. *Journal of Crystal Growth* 1979, 46, (1), 7-9.

(6) Young, S. W., Mechanical stimulus to crystallization in supercooled liquids. *Journal of the American Chemical Society* 1911, 33, 148-162.

(7) Young, S. W.; Cross, R. J., The mechanical stimulus to crystallization. II. *Journal of the American Chemical Society* 1911, 33, 1375-1388.

(8) Young, S. W.; Van Sicklen, W. J., The mechanical stimulus to crystallization. *Journal of the American Chemical Society* 1913, 35, 1067-1078.

(9) Earl of Berkeley, Solubility and supersolubility from the osmotic standpoint. *Philosophical Magazine* 1912, 24, (140), 254-268.

(10) Taleb, M.; Didierjean, C.; Jelsch, C.; Mangeot, J. P.; Capelle, B.; Aubry, A., Crystallization of proteins under an external electric field. *Journal of Crystal Growth* 1999, 200, (3-4), 575-582.

(11) Sazaki, G.; Yoshida, E.; Komatsu, H.; Nakada, T.; Miyashita, S.; Watanabe, K., Effects of a magnetic field on the nucleation and growth of protein crystals. *Journal of Crystal Growth* 1997, 173, (1-2), 231-234.

(12) Zaccaro, J.; Matic, J.; Myerson, A. S.; Garetz, B. A., Nonphotochemical, laser-induced nucleation of supersaturated aqueous glycine produces unexpected gamma-polymorph. *Crystal Growth & Design* 2001, 1, (1), 5-8.

(13) Delucas, L. J.; Suddath, F. L.; Snyder, R.; Naumann, R.; Broom, M. B.; Pusey, M.; Yost, V.; Herren, B.; Carter, D.; Nelson, B.; Meehan, E. J.; McPherson, A.; Bugg, C. E., Preliminary Investigations Of Protein Crystal-Growth Using The Space-Shuttle. *Journal of Crystal Growth* 1986, 76, (3), 681-693.

(14) Ruecroft, G.; Hipkiss, D.; Ly, T.; Maxted, N.; Cains, P. W., Sonocrystallization: The use of ultrasound for improved industrial crystallization. *Organic Process Research & Development* 2005, 9, (6), 923-932.

(15) Mullin, J. W., *Crystallization*. 4th ed.; Heineman: 2002.

(16) Parambil, J. V.; Schaepertoens, M.; Williams, D. R.; Heng, J. Y. Y., Effects of Oscillatory Flow on the Nucleation and Crystallization of Insulin. *Crystal Growth & Design* 2011, 11, (10), 4353-4359.

(17) Penkova, A.; Pan, W. C.; Hodjaoglu, F.; Vekilov, P. G., Nucleation of protein crystals under the influence of solution shear flow. *Interdisciplinary Transport Phenomena in the Space Sciences* 2006, 1077, 214-231.

(18) Roberts, M. M.; Heng, J. Y. Y.; Williams, D. R., Protein Crystallization by Forced Flow through Glass Capillaries: Enhanced Lysozyme Crystal Growth. *Crystal Growth & Design* 2010, 10, (3), 1074-1083.

(19) Chen, D. L.; Gerdts, C. J.; Ismagilov, R. F., Using microfluidics to observe the effect of mixing on nucleation of protein crystals. *Journal of the American Chemical Society* **2005,** 127, (27), 9672-9673..

(20) Keller, A., Polymer Crystals. *Reports on Progress in Physics* 1968, 31, 623-&.

(21) Mackley, M. R.; Keller, A., Flow Induced Polymer-Chain Extension And Its Relation To Fibrous Crystallization. *Philosophical Transactions of the Royal Society a-Mathematical Physical and Engineering Sciences* 1975, 278, (1276), 29-+.

(22) Jawor-Baczynska, A.; Sefcik, J.; Moore, B. D., 250 nm Glycine-Rich Nanodroplets Are Formed on Dissolution of Glycine Crystals But Are Too Small To Provide Productive Nucleation Sites. *Crystal Growth & Design* 2013, 13, (2), 470-478.

(23) Liang, K. P.; White, G.; Wilkinson, D.; Ford, L. J.; Roberts, K. J.; Wood, W. M. L., An examination into the effect of stirrer material and agitation rate on the nucleation of L-glutamic acid batch crystallized from supersaturated aqueous solutions. *Crystal Growth & Design* 2004, 4, (5), 1039-1044.

(24) Liu, J.; Rasmuson, A. C., Influence of Agitation and Fluid Shear on Primary Nucleation in Solution. *Crystal Growth & Design* 2013, 13, (10), 4385-4394.

(25) Sypek, K.; Burns, I. S.; Florence, A. J.; Sefcik, J., In Situ Monitoring of Stirring Effects on Polymorphic Transformations during Cooling Crystallization of Carbamazepine. *Crystal Growth & Design* 2012, 12, (10), 4821-4828.

(26) Reis, N. M.; Chirgadze, D. Y.; Blundell, T. L.; Mackley, M. R., The effect of protein-precipitant interfaces and applied shear on the nucleation and growth of lysozyme crystals. *Acta Crystallographica Section D-Biological Crystallography* 2009, 65, 1127-1139.

(27) Ackerson, B. J.; Pusey, P. N., Shear-Induced Order In Suspensions Of Hard-Spheres. *Physical Review Letters* 1988, 61, (8), 1033-1036.

(28) Haw, M. D.; Poon, W. C. K.; Pusey, P. N., Direct observation of oscillatory-shear-induced order in colloidal suspensions. *Physical Review E* 1998, 57, (6), 6859-6864.

(29) Amos, R. M.; Rarity, J. G.; Tapster, P. R.; Shepherd, T. J.; Kitson, S. C., Fabrication of large-area face-centered-cubic hard-sphere colloidal crystals by shear alignment. *Physical Review E* 2000, 61, (3), 2929-2935.

(30) Palberg, T.; Monch, W.; Schwarz, J.; Leiderer, P., Grain-Size Control In Polycrystalline Colloidal Solids. *Journal of Chemical Physics* 1995, 102, (12), 5082-5087.

(31) Butler, S.; Harrowell, P., Kinetics Of Crystallization In A Shearing Colloidal Suspension. *Physical Review E* 1995, 52, (6), 6424-6430.

(32) Blaak, R.; Auer, S.; Frenkel, D.; Lowen, H., Homogeneous nucleation of colloidal melts under the influence of shearing fields. *Journal of Physics-Condensed Matter* 2004, 16, (38), S3873-S3884.

(33) Taylor, G. I., Stability of a viscous liquid contained between two rotating cylinders. Philosophical Transactions of the Royal Society of London Series a-Containing Papers of a Mathematical or Physical Character 1923, 223, 289-343.

(34) Devine, W.; Lowe, B. M., Viscosity B-Coefficients At 15 And 25 Degrees C For Glycine, Beta-Alanine, 4-Amino-Butyric Acid, And 6-Amino-Hexanoic Acid In Aqueous Solution. Journal of the Chemical Society a -Inorganic Physical Theoretical 1971, (13), 2113-&.

(35) Green, D.; Perry, R., Perry's Chemical Engineers' Handbook. 8 ed.; McGraw-Hill Professional: 2007.

(36) Jelinska Kazimierczuk, M.; Szydlowski, J., Isotope effect on the solubility of amino acids in water. *Journal of Solution Chemistry* 1996, 25, (12), 1175-1184.

(37) Dowling, R.; Davey, R. J.; Curtis, R. A.; Han, G. J.; Poornachary, S. K.; Chow, P. S.; Tan, R. B. H., Acceleration of crystal growth rates: an unexpected effect of tailor-made additives. *Chemical Communications* 2010, 46, (32), 5924-5926.

(38) Jiang, S. F.; ter Horst, J. H., Crystal Nucleation Rates from Probability Distributions of Induction Times. *Crystal Growth & Design* 2011, 11, (1), 256-261.

(39) Kadam, S. S.; Kramer, H. J. M.; ter Horst, J. H., Combination of a Single Primary Nucleation Event and Secondary Nucleation in Crystallization Processes. *Crystal Growth & Design* 2011, 11, (4), 1271-1277.

(40) Kadam, S. S.; Kulkarni, S. A.; Ribera, R. C.; Stankiewicz, A. I.; ter Horst, J. H.; Kramer, H. J. M., A new view on the metastable zone width during cooling crystallization. *Chemical Engineering Science* 2012, 72, 10-19.

(41) Limpert, E.; Stahel, W. A.; Abbt, M., Log-normal distributions across the sciences: Keys and clues. *Bioscience* 2001, 51, (5), 341-352.

(42) Galkin, O.; Vekilov, P. G., Direct determination of the nucleation rates of protein crystals. *Journal of Physical Chemistry B* 1999, 103, (49).

(43) Kulkarni, S. A.; Kadam, S. S.; Meekes, H.; Stankiewicz, A. I.; ter Horst, J. H., Crystal Nucleation Kinetics from Induction Times and Metastable Zone Widths. *Crystal Growth & Design* 2013, 13, (6), 2435-2440.

(44) Press, W. H.; Teukolsky, S. A.; Vetterling, W. T.; Flannery, B. P., *Numerical Recipes in Fortran 77*. ed.; Cambridge University Press: New York, 2006.

(45) O'Neill, K. P.; Grinfeld, M.; Lamb, W.; Mulheran, P. A., Gap-size and capture-zone distributions in one-dimensional point-island nucleation and growth simulations: Asymptotics and models. *Physical Review E* 2012, 85, (2), 8.

For Table of Contents Use Only.

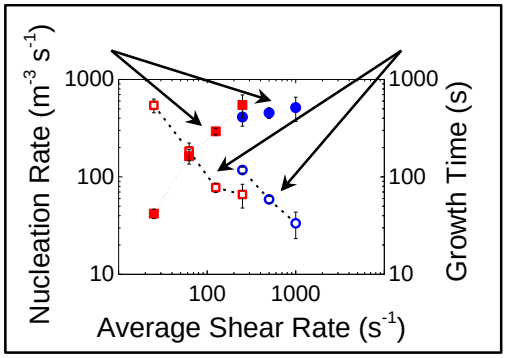

Graph showing that the primary nucleation rate increases and at the same time, the growth time decreases with increasing average shear rate.